Research Square

Preprints are preliminary reports that have not undergone peer review.
They should not be considered conclusive, used to inform clinical practice,
or referenced by the media as validated information.

An Integrated Computational Assessment of the Structural, Electronic, and Predicted Pharmacokinetic Properties of Ten Benzodiazepines

Moshiur Rahman

muhammadmoshiurrahman9007@gmail.com

Jahangirnagar University

Md. Tarikul Islam

Comilla University

Shohanul Islam Sarker

Comilla University

Shamim Ahammad

Comilla University

Abir Hossen Tanvir

Govt. Hazi Mohammad Mohsin College

Pronob Das

Dhaka College

Research Article

Keywords: Benzodiazepines, Density functional theory, Molecular docking, Molecular dynamics simulations, ADMET prediction

Posted Date: November 13th, 2026

DOI: https://doi.org/10.21203/rs.3.rs-11565880/v1

License: This work is licensed under a Creative Commons Attribution 4.0 International License.
Read Full License

Additional Declarations: No competing interests reported.

An Integrated Computational Assessment of the Structural, Electronic, and Predicted Pharmacokinetic Properties of Ten Benzodiazepines

Moshiur Rahman[1,α,*], Md.Tarikul Islam[2,α], Shohanul Islam Sarker[2], Shamim Ahammad[2], Abir Hossen Tanvir[3], Pronob Das[4].

[1]Department of Biochemistry and Molecular Biology, Faculty of Biological Sciences, Jahangirnagar University, Savar, Dhaka 1342, Bangladesh.

[2]Department of Pharmacy, Comilla University, Cumilla 3506, Bangladesh

[3]Department of Chemistry, Govt. Hazi Mohammad Mohsin College, Chattogram 4000, Bangladesh

[4]Department of Chemistry, Dhaka College, New Market, Dhaka 1205

*Corresponding author e-mail: muhammadmoshiurrahman9007@gmail.com

[α]These authors contributed equally to this work.

Abstract

Benzodiazepines (BZDs) are widely used to manage anxiety, insomnia, seizures, and other neurological conditions through modulation of gamma-aminobutyric acid type A (GABA-A) receptor-mediated inhibition. Despite their therapeutic utility, prolonged use may be associated with tolerance, dependence, and adverse effects. This study presents an integrated computational assessment of ten BZDs, combining density functional theory (DFT), molecular docking, molecular dynamics (MD) simulations, and predicted pharmacokinetic and biological activity profiling. Molecular geometries were optimized at the B3LYP/6-311G+(d,p) level, and thermodynamic properties, frontier molecular orbitals, dipole moments, and molecular

electrostatic potentials were analyzed. Molecular docking was conducted using the human GABA-A receptor structure (PDB ID: 6HUO), focusing on the isolated α1 subunit (Chain D). Three prioritized protein–ligand complexes were subsequently examined through 100-ns MD simulations to characterize their structural behavior and interaction patterns. Predicted absorption, distribution, metabolism, excretion, and toxicity (ADMET) properties and PASS-based activity profiles were also evaluated. The compounds exhibited differences in frontier molecular orbital energies and related electronic descriptors. Docking suggested favorable poses within the selected α1-subunit region, while MD simulations provided additional insights into the behavior of the prioritized complexes. PASS and ADMET analyses generated hypotheses concerning potential biological activities and pharmacokinetic characteristics. These findings provide comparative computational insights into the studied BZDs; however, experimental validation is required, and the isolated-subunit docking results do not establish binding at the canonical BZD site or demonstrate receptor modulation or clinical effects.

Keywords: Benzodiazepines; Density functional theory; Molecular docking; Molecular dynamics simulations; ADMET prediction.

Introduction

BZDs are widely used central nervous system (CNS) medications for the management of anxiety, insomnia, seizures, and other neurological conditions. They act as positive allosteric modulators of γ-aminobutyric acid type A (GABA-A) receptors, enhancing GABA-mediated inhibitory neurotransmission by increasing the frequency of chloride channel opening [1–6]. GABA-A receptors are pentameric ligand-gated ion channels composed of five subunits arranged around a central chloride-conducting pore. A common receptor composition consists of two α, two β, and one γ subunit. GABA binds at extracellular β–α subunit interfaces, whereas classical BZDs interact with an allosteric binding pocket formed at the α–γ subunit interface. This modulation

of inhibitory neurotransmission underlies the sedative, hypnotic, anxiolytic, and anticonvulsant effects associated with BZDs [7–9].

Although BZDs are generally considered safer than several older sedative-hypnotic agents, their clinical use is associated with important safety concerns, particularly among elderly individuals. Prolonged use may contribute to falls, cognitive impairment, tolerance, physical dependence, and withdrawal symptoms. Other adverse effects include drowsiness, disorientation, and impaired psychomotor function. Consequently, their use is generally recommended for short-term or carefully monitored treatment, depending on the clinical indication and individual patient characteristics [10–12]. These concerns emphasize the importance of investigating the molecular and pharmacokinetic characteristics of individual BZDs to improve the understanding of their structural properties and potential biological activities.

Despite their extensive clinical use, BZDs exhibit considerable structural diversity, including differences in their fused-ring systems, substituents, heteroatom composition, and physicochemical properties. Such structural variations may influence their electronic characteristics, predicted protein interactions, conformational behavior, and pharmacokinetic profiles. Previous computational investigations have examined individual aspects of benzodiazepine pharmacology, including receptor interactions, electronic properties, and pharmacokinetics. However, an integrated comparative investigation combining quantum chemical calculations, molecular docking, MD simulations, biological activity prediction, and ADMET assessment can provide complementary information across different molecular endpoints. This approach may help characterize structural differences among BZDs and generate hypotheses concerning their molecular interactions and potential biological properties.

The present study investigated ten clinically used benzodiazepines: temazepam (TMZ), chlordiazepoxide (CDP), flurazepam (FZP), midazolam (MDZ), oxazepam (OXA),

clorazepate (CZP), clobazam (CBZ), estazolam (ESZ), clonazepam (CLZ), and nitrazepam (NZP). These compounds were selected to represent a chemically diverse group of benzodiazepine derivatives with established clinical applications in neurological and psychiatric treatment. Their structural differences provide a basis for comparing molecular descriptors, predicted interactions, and pharmacokinetic characteristics within a common computational framework. The inclusion of conventional BZDs alongside structurally distinct derivatives, such as clobazam, further enables the investigation of differences associated with variations in molecular scaffolds and functional groups.

The human GABA-A receptor cryo-electron microscopy structure (PDB ID: 6HUO) was used as the structural framework for the molecular docking investigation. Chain D, corresponding to the α1 subunit, was isolated and employed as the receptor model to examine the predicted interactions of the selected compounds within a consistently defined protein environment. The docking grid was centered on the co-crystallized ligand alprazolam, allowing the ligand poses to be evaluated within the corresponding region of the isolated subunit. However, because the classical benzodiazepine-binding pocket is formed at the α1–γ2 subunit interface, the isolated α1-subunit model does not fully represent the native intersubunit binding environment. Accordingly, the docking results and subsequent MD simulations are interpreted as exploratory computational observations of ligand interactions with the modeled α1 subunit rather than direct evidence of binding at the complete canonical benzodiazepine site or receptor modulation.

To characterize the selected compounds at complementary molecular levels, density functional theory (DFT)-based quantum chemical calculations were performed using the B3LYP/6-311G+(d,p) method to investigate their thermodynamic and electronic properties, including frontier molecular orbital energies, HOMO–LUMO energy gaps, dipole moments, and molecular electrostatic potentials. Chemical hardness, softness, and chemical potential were

derived from the frontier orbital energies to provide comparative descriptors of electronic structure and reactivity. Molecular docking was subsequently employed to investigate the predicted binding poses, docking scores, and non-covalent interactions of the BZDs with the isolated α1-subunit model. The three compounds selected for further investigation, CZP, NZP, and OXA, were subjected to 100 ns MD simulations to examine their conformational behavior, protein and ligand RMSD, residue-level fluctuations, hydrogen-bonding patterns, radius of gyration, solvent-accessible surface area, and protein–ligand interaction profiles. These analyses provided complementary information regarding the dynamic characteristics of the modeled complexes beyond their initial docking poses.

In addition, PASS was employed to explore the potential biological activity profiles of the selected BZDs based on their chemical structures. The predicted probabilities of activity (Pa) and inactivity (Pi) were examined for pharmacological activities relevant to CNS function, including anxiolytic, anticonvulsant, antiepileptic, muscle-relaxant, and GABA receptor-associated activities. PASS analysis was incorporated to compare the predicted biological activity spectra of the compounds and identify additional hypotheses for further investigation. ADMET prediction was also conducted to characterize their computationally estimated absorption, distribution, metabolism, excretion, and toxicity-related properties. Together, these complementary analyses enabled the comparative assessment of electronic properties, predicted protein interactions, dynamic behavior, potential biological activities, and pharmacokinetic characteristics.

Overall, this study presents an integrated computational characterization of ten BZDs using DFT calculations, molecular docking, MD simulations, PASS prediction, and ADMET assessment. By examining these compounds across multiple computational endpoints, the investigation aims to identify structural and electronic differences, characterize their predicted interactions with the isolated GABA-A receptor α1 subunit, and evaluate their predicted

biological activity and pharmacokinetic profiles. The findings may provide comparative molecular information for interpreting benzodiazepine structure–activity relationships and generating hypotheses for future structural and experimental pharmacological investigations. Importantly, the study is intended to complement existing research rather than establish receptor activation, canonical-site binding affinity, subtype selectivity, or clinical efficacy solely from computational predictions.

Methods and Materials

Geometry optimization

The chemical structures of all selected drugs were retrieved from the PubChem online structure database (https://pubchem.ncbi.nlm.nih.gov/) [13]. To determine the most stable and energetically favorable conformations, MD conformational searches were conducted using the amber force field, implemented via Gabedit (version 2.5.1) software [14]. Geometry optimizations were carried out using the Gaussian 16 software [15]. Density Functional Theory (DFT) was applied, employing a hybrid exchange-correlation functional combining Becke's three-parameter exchange and Lee–Yang–Parr correlation (B3LYP), together with the triple-zeta 6-311G+(d, p) basis set [16]. The HOMO and LUMO energies, as part of the frontier molecular orbital (FMO) analysis, were computed employing the same computational method [17]. Using the calculated εHOMO and εLUMO values, key electronic properties such as the energy gap (**ΔE**), softness (**S**), hardness (**η**), and chemical potential (**μ**) were derived using standard formulas:

$$\mathbf{\Delta E} = \varepsilon LUMO - \varepsilon HOMO$$

$$\mathbf{S} = \frac{1}{\varepsilon LUMO - \varepsilon HOMO}$$

$$\boldsymbol{\eta} = \frac{\varepsilon LUMO - \varepsilon HOMO}{2}$$

147 $$\boldsymbol{\mu} = \frac{\varepsilon LUMO + \varepsilon HOMO}{2}$$

148 Protein and ligand preparation

149 The three-dimensional cryo-EM structure of the human full-length heteromeric α1β3γ2L
150 GABAA_AA receptor in complex with alprazolam, GABA, and megabody Mb38 (PDB ID:
151 6HUO; resolution: 3.26 Å) was retrieved from the Protein Data Bank [18]. Only Chain D,
152 corresponding to the α1 subunit, was retained for molecular docking and interaction analysis.
153 Chain D was selected to investigate the interactions of the ten BZDs with the α1 subunit, which
154 contributes to the classical benzodiazepine-binding interface in the assembled receptor.
155 Focusing on this chain reduced structural complexity and computational overhead while
156 enabling comparative analysis of ligand–residue interactions within the selected subunit. The
157 remaining protein chains (A, B, C, E, F, G, H, I, J, and K), co-crystallized ligands, heteroatoms,
158 and water molecules were removed using BIOVIA Discovery Studio Visualizer (BIOVIA,
159 2017) [19,20]. The structure was subsequently energy-minimized using Swiss-PdbViewer (v4.1.0)
160 prior to docking[21] .

161 Validation of the Molecular Docking Protocol

162 A redocking procedure was performed to assess the reliability of the molecular docking
163 protocol before docking the test compounds. The co-crystallized ligand alprazolam (ALP) was
164 removed from the receptor structure (PDB ID: 6HUO; Chain D) and re-docked into the selected
165 binding site using the same docking parameters applied to the test compounds. The re-docked
166 pose was superimposed onto the crystallographic conformation using PyMOL, and the root-
167 mean-square deviation (RMSD) between the corresponding heavy atoms was calculated. An
168 RMSD value of ≤2.0 Å was considered acceptable for reproducing the experimentally
169 determined ligand-binding pose and validating the docking protocol [22].
170

Molecular docking analysis

Following validation of the docking protocol, the geometry-optimized structures of ten benzodiazepine (BZD) drugs were used as ligands, while the energy-minimized receptor structure (6HUO, Chain D) was used as the macromolecular target. AutoDock Tools (version 1.5.7) was employed to convert the receptor and ligand structures into PDBQT format. Molecular docking was performed within the validated binding region using a grid box centered at X = 153.788, Y = 162.829, and Z = 160.817 Å, with dimensions of 30 × 30 × 30 $Å^3$ to encompass the selected binding region [23]. For each ligand, the pose with the lowest predicted binding free energy was selected for subsequent analysis. Protein–ligand interactions were analyzed and visualized using BIOVIA Discovery Studio Visualizer (version 21.1.0.20298) [19].

MD Simualtion

MD simulations were performed to investigate the dynamic behavior and structural stability of the selected protein–ligand complexes. Simulations were conducted for 100 ns using Desmond (Schrödinger) under a Linux environment [24]. The systems were solvated using the SPC water model [25] and neutralized with Na^+ and Cl^- ions at a concentration of 0.15 M. An orthorhombic simulation box with a 10 Å buffer surrounding the solute was generated, and periodic boundary conditions were applied. Simulations were performed using the OPLS4 force field under the isothermal–isobaric (NPT) ensemble at 298 K and 1.01325 bar. Trajectory frames were recorded at 100 ps intervals [26]. These simulations enabled the assessment of protein–ligand complex stability and conformational dynamics under the specified simulation conditions.

SMILES preparation and ADMET prediction

SMILES representations of the selected FDA-approved benzodiazepine drugs were obtained using the Online SMILES Translator and Structure File Generator server of the National Cancer Institute (NCI) (https://cactus.nci.nih.gov/translate/). As the selected compounds are

established FDA-approved drugs, ADMET analysis was performed primarily to characterize and comparatively evaluate their predicted absorption, distribution, metabolism, excretion, and toxicity-related properties within the present computational study, rather than to assess their clinical suitability. The ADMET profiles were predicted using the admetSAR 1.0 web server (https://lmmd.ecust.edu.cn/admetsar1). The predicted parameters were comparatively examined across the benzodiazepine series to characterize their pharmacokinetic and toxicity-related profiles [27].

PASS Prediction

The PASS prediction tool was used to evaluate the broad range of biological activities of the selected FDA-approved drugs, providing computational insights into their potential biological effects. The SMILES of the selected drugs were submitted to the PASS online server (http://www.way2drug.com/passonline) to predict their potential biological activities [28]. The results provided probability of activity (Pa), showing the predicted likelihood of a compound exhibiting a particular biological activity, with values ranging from zero to one.

Results

Analysis of thermodynamic properties

Thermodynamic and electronic properties provide useful information about the molecular characteristics of BZDs, including their relative energetic states, polarity, and potential reactivity. Key parameters such as Gibbs free energy (**ΔG**), enthalpy (**ΔH**), and dipole moment (**μ**) were evaluated to characterize the studied compounds [29,30]. The calculated energy values should be interpreted as properties of the individual molecular systems rather than direct indicators of receptor-binding strength.

Among the analyzed BZDs, FZP showed the most negative calculated total energy (−1613.578 Hartree), followed by CLZ (−1427.754 Hartree), whereas NZP showed the least negative value among the studied compounds. These differences primarily reflect the overall electronic energy of molecules with different atomic compositions and structures and should not be interpreted directly as differences in molecular stability or receptor-binding affinity.

Dipole moment (**μ**) provides information about the overall charge distribution and polarity of a molecule and may influence its electrostatic environment and intermolecular interactions [31]. ESZ exhibited the highest dipole moment (5.71 Debye), whereas CLZ showed the lowest value (0.56 Debye) (Figure 2B). The remaining compounds, including TMZ, CDP, CBZ, FZP, MDZ, CZP, OXA, and NZP, displayed intermediate dipole moments. These differences indicate variation in molecular polarity and charge distribution but do not, by themselves, establish stronger or weaker receptor interactions.

Molecular Orbital Analysis

Frontier molecular orbitals (FMOs), particularly the highest occupied molecular orbital (HOMO) and lowest unoccupied molecular orbital (LUMO), provide useful information about the electronic characteristics and chemical reactivity of molecules. The HOMO is generally associated with electron-donating ability, whereas the LUMO is associated with electron-accepting ability [32,33]. The HOMO–LUMO energy gap represents the energy difference between these orbitals and is commonly used as an indicator of molecular reactivity and kinetic stability [34,35]. A larger gap generally corresponds to lower chemical reactivity, whereas a smaller gap may indicate greater chemical reactivity.

As shown in Figure 3, CDP exhibited the smallest HOMO–LUMO gap (2.81 eV) among the studied BZDs, suggesting comparatively greater predicted chemical reactivity. In contrast, CBZ showed the largest gap (5.05 eV), indicating comparatively lower predicted reactivity and greater kinetic stability. Chemical hardness (**η**) and softness (**S**) were also derived from the

HOMO and LUMO energies [35]. Higher hardness generally indicates greater resistance to electronic deformation, whereas higher softness is associated with greater electronic polarizability and reactivity [32]. TMZ, CZP, OXA, MDZ, and FZP exhibited relatively lower softness values (0.21–0.25 eV), whereas NZP showed the highest softness value (0.494 eV), indicating comparatively greater predicted electronic reactivity. These FMO-derived properties provide insights into the electronic behavior of the studied BZDs but do not, by themselves, establish receptor-binding strength or biological efficacy.

Molecular electrostatic potential (MEP) analysis

Molecular electrostatic potential (MEP) mapping provides useful information about the charge distribution of a molecule and helps identify regions that may participate in electrostatic interactions, hydrogen bonding, and molecular recognition [17]. In the MEP maps, red regions represent areas of relatively negative electrostatic potential, which may favor interactions with electrophilic species, whereas blue regions indicate relatively positive potential and may favor interactions with nucleophilic species [36,37]. Among the studied BZDs, NZP exhibited the highest negative electrostatic potential around its oxygen atoms (−0.066 a.u.), represented by the deepest red region, while its highest positive potential was observed around hydrogen atoms (+0.066 a.u.), represented by the deepest blue region. CLZ and CZP showed the next highest negative potential values around their oxygen atoms, at −0.064 and −0.063 a.u., respectively, with corresponding maximum positive potential values of +0.064 and +0.063 a.u. around hydrogen atoms. These variations indicate differences in the electrostatic charge distribution of the studied compounds. The MEP maps of NZP, CLZ, and CZP are presented in **Figure 4**.

Validation analysis of the Molecular Docking Protocol

The crystallographic orientation of the redocked alprazolam (ALP) was comparable to its original conformation, with a heavy-atom RMSD of 1.89 Å between the two structures (**Figure**

5). As the RMSD was below the commonly used threshold of 2.0 Å, the result indicated good reproducibility of the docking procedure for reproducing the ALP pose within the selected docking region of the isolated α1-subunit model. However, this validation does not establish the representation of the canonical benzodiazepine-binding site, as the α1–γ2 subunit interface was not retained in the docking model.

BZD drugs' docking scores and interactions with 6HUO

Molecular docking was performed to explore the potential interactions of BZDs with the isolated α1 subunit (Chain D) of the human GABA-A receptor (PDB ID: 6HUO), focusing on predicted docking scores and ligand positioning within the selected docking region. The GABA-A receptor is an important pharmacological target in neuropharmacology and psychiatric treatment [3,38]. The docking protocol was evaluated by extracting and re-docking the co-crystallized ligand alprazolam (ALP) into the prepared α1-subunit model. The minor positional deviation between the original and re-docked ALP conformations indicated reproducibility of ligand placement within the isolated-subunit model [38,39]. However, this validation does not establish canonical benzodiazepine-site binding, as the α1–γ2 subunit interface was not retained. Docking scores for all compounds are presented in **Table 1**.

Using ALP as the reference compound (−7.5 kcal/mol), several BZDs showed comparable or favorable predicted docking scores, including OXA (−7.3 kcal/mol), NZP (−7.1 kcal/mol), CZP (−6.9 kcal/mol), ESZ (−6.8 kcal/mol), and CDP (−6.7 kcal/mol). Other compounds in the lower docking-score range included FZP (−6.2 kcal/mol) and CBZ (−6.1 kcal/mol) [40]. Analysis of the docking poses revealed various noncovalent contacts between the ligands and residues within the selected α1-subunit region. Several BZDs formed conventional hydrogen bonds involving residues such as SER205, TYR210, and PHE100. OXA, NZP, and CZP formed relatively short hydrogen-bond contacts (<2.3 Å), which may contribute to their predicted docking scores [3,41,42].

Aromatic interactions, including π–π contacts involving TYR210, TYR160, and PHE100, were also observed with the aromatic rings of several ligands. Hydrophobic interactions, including alkyl and π-alkyl contacts, were particularly observed for CBZ, including contacts with residues such as PRO525 and GLU522. Additional interactions, including halogen and carbon–hydrogen contacts, were observed less frequently. Overall, the docking results indicate that differences in hydrogen bonding, aromatic contacts, and hydrophobic interactions may contribute to variation in the predicted docking scores among the studied BZDs. These findings describe computationally predicted interaction patterns within the isolated α1-subunit model and should not be interpreted as direct evidence of canonical benzodiazepine-site binding or receptor modulation.

SAR on binding affinity

The docking scores of the selected BZDs against the D chain of the 6HUO protein were ranked as follows: OXA (−7.3 kcal/mol) > NZP (−7.1 kcal/mol) > CZP (−6.9 kcal/mol) > ESZ (−6.8 kcal/mol) ≈ TMZ (−6.8 kcal/mol) ≈ CDP (−6.8 kcal/mol) ≈ MDZ (−6.8 kcal/mol) > CLZ (−6.6 kcal/mol) > CBZ (−6.4 kcal/mol) > FZP (−6.2 kcal/mol), with ALP showing a docking score of −7.5 kcal/mol. Structural differences among the BZDs, including substitutions at the N1, C3, C5, and C7 positions, may contribute to differences in their predicted interaction patterns and docking scores.

ALP, the co-crystallized reference ligand, showed the most favorable docking score among the analyzed compounds. Its triazolo-fused ring system may contribute to its observed pose through aromatic and other noncovalent interactions within the selected docking region. OXA, which showed the most favorable docking score among the studied BZDs, contains a hydroxyl (−OH) group at the C3 position that may facilitate hydrogen-bonding interactions with residues in the docking region. NZP, bearing a nitro ($-NO_2$) group at C7, exhibited a strong electron-withdrawing substituent that may influence its electrostatic interactions and contribute to its

predicted docking score. CZP contains a carboxyl (−COOH) group at C3, which may participate in hydrogen-bonding and electrostatic interactions.

ESZ, featuring a fused triazole ring, may benefit from its aromatic and electronically delocalized structure, which could contribute to its predicted interaction pattern. TMZ and CDP exhibited moderate docking scores; TMZ contains a hydroxyl group at C3, whereas CDP contains an N4-oxide (−N→O) moiety that increases molecular polarity and may influence its interactions within the docking region.

MDZ, despite containing an imidazole-fused ring, showed a slightly less favorable docking score, which may be related to differences in its orientation or steric environment within the selected region. CLZ, containing a nitro group at C7, showed an intermediate docking score. CBZ, a 1,5-benzodiazepine derivative, displayed a less favorable score, potentially reflecting differences in ring geometry and aromatic contacts. FZP, bearing an N1-alkyl substitution, showed the least favorable docking score among the studied compounds, although the contribution of this substituent to the predicted pose cannot be established from docking alone. Overall, the observed variation in docking scores may reflect differences in molecular structure, hydrogen-bonding capacity, aromatic character, polarity, and steric features among the studied BZDs [43,44]. These findings represent computationally predicted interaction patterns within the isolated α1-subunit model and should not be interpreted as direct evidence of canonical benzodiazepine-site affinity or receptor modulation.

MD simulation analysis

A 100 ns MD simulation was conducted using the Desmond module within the Schrödinger suite. The Simulation Interaction Diagram (SID) was employed to comprehensively analyze the dynamic behavior of the complexes, including protein and ligand RMSD, residue flexibility (RMSF), hydrogen bond formation, radius of gyration (Rg), solvent-accessible surface area

(SASA), and detailed protein–ligand as well as ligand–protein interaction profiles throughout the simulation trajectory.

Protein RMSD Analysis

To examine the conformational behavior of the isolated α1-subunit model in complex with three selected BZDs (CZP, NZP, and OXA), 100 ns MD simulations were performed, and the root mean square deviation (RMSD) of each complex was analyzed (Figure 6). The CZP-bound complex showed an initial adjustment during the first 10 ns, with RMSD values ranging from 1.91 to 8.51 Å (average 4.67 ± 1.15 Å), followed by a relatively consistent trajectory until approximately 80 ns. The fluctuations observed toward the end of the simulation may reflect conformational adjustments in flexible regions of the protein [45].

The NZP-bound complex reached an apparently stable trajectory within approximately 5 ns, with RMSD values ranging from 2.26 to 6.31 Å (average 4.31 ± 0.95 Å) throughout the simulation. The relatively consistent trajectory suggests that the overall conformation of the isolated α1-subunit model was maintained during the simulation. Persistent hydrogen-bonding interactions observed during the simulation may have contributed to the observed interaction pattern. The OXA-bound complex showed RMSD values between 1.83 and 7.04 Å (average 4.57 ± 0.74 Å). The trajectory remained relatively consistent until approximately 70 ns, followed by moderate fluctuations that may reflect transient conformational adjustments or changes in ligand orientation [46].

Overall, all three complexes maintained their overall structural behavior throughout the 100 ns simulations, although differences in RMSD profiles were observed. NZP showed the lowest average RMSD among the three complexes, indicating comparatively lower overall conformational deviation during the simulation. These findings provide insight into the dynamic behavior of the prioritized ligand–α1-subunit complexes; however, RMSD alone does not establish binding affinity or receptor activity.

Ligand RMSD Analysis

Ligand RMSD analysis was performed to examine the conformational behavior of the three prioritized compounds during the 100 ns MD simulations (Figure 6). Lower ligand RMSD values generally indicate smaller deviations from the reference conformation, whereas larger fluctuations may reflect conformational changes or changes in ligand orientation during the simulation. NZP showed the lowest average RMSD among the three ligands, ranging from 2.482 to 7.095 Å (average 5.116 ± 0.538 Å), with a comparatively consistent trajectory throughout the simulation. CZP exhibited RMSD values ranging from 2.590 to 37.927 Å (average 13.793 ± 3.779 Å), showing relatively consistent behavior until approximately 70 ns followed by increased fluctuations during the later phase. OXA displayed the largest deviations, with RMSD values ranging from 2.470 to 94.192 Å (average 25.590 ± 22.960 Å), particularly after approximately 60 ns, indicating substantial changes in ligand conformation or orientation relative to the initial pose.

Overall, NZP exhibited comparatively lower conformational deviation during the simulation, whereas CZP and OXA showed greater fluctuations. These differences provide insight into the dynamic behavior of the ligands within the simulated isolated α1-subunit model. However, ligand RMSD alone cannot establish binding affinity, binding persistence, or ligand dissociation; such interpretations require consideration of additional trajectory-based analyses, including protein–ligand contacts, hydrogen-bond occupancy, ligand–protein distances, and interaction patterns.

Protein RMSF Analysis

The flexibility and residue-level dynamics of the isolated α1-subunit model in complex with CZP, NZP, and OXA were investigated using root mean square fluctuation (RMSF) analysis during the 100 ns MD simulations. RMSF measures the average positional fluctuation of

individual residues around their mean positions and provides information on local protein flexibility during the simulation [47,48].

Most residues showed relatively low fluctuations, generally below 2 Å, across the three complexes. The mean RMSF values were 1.978 Å for CZP, 2.206 Å for NZP, and 1.826 Å for OXA. These values indicate that most regions of the isolated α1-subunit model exhibited limited residue-level fluctuations throughout the simulations. The maximum RMSF values were 9.516 Å for CZP, 9.364 Å for NZP, and 8.182 Å for OXA, suggesting that the larger deviations were localized to specific regions rather than distributed throughout the protein. Such localized fluctuations can occur in flexible loops, surface-exposed segments, or terminal regions [49,50].

The CZP complex showed the highest fluctuation at THR310 (9.516 Å), with neighboring residues LYS308 (9.174 Å), PHE311 (8.648 Å), and ASN312 (7.719 Å) also displaying elevated mobility. Similarly, the NZP complex exhibited pronounced fluctuations around THR310 (9.364 Å), while LYS308 (8.346 Å), PHE311 (8.444 Å), and ASN312 (7.165 Å) showed comparable mobility. In the OXA complex, the mean RMSF was comparatively lower (1.826 Å), although notable fluctuations were observed at LYS308 (8.182 Å) and GLY307 (6.356 Å). The recurring RMSF peaks across the TRP305–ASN312 region, particularly around LYS308–THR310, indicate that this segment represents a comparatively flexible region of the simulated α1-subunit model.

Overall, the RMSF profiles indicate that residue-level fluctuations were largely localized to specific regions, while most residues exhibited relatively limited mobility. The observed flexibility may contribute to local conformational adjustments during ligand-bound simulations; however, RMSF alone cannot establish ligand-induced allosteric effects, binding-site breathing, or mechanisms of ligand attachment or dissociation [51,52].

Radius of Gyration (Rg) Analysis

Rg was analyzed to examine the overall compactness of the simulated protein–ligand complexes during the 100 ns MD simulations. Rg describes the distribution of protein atoms around their center of mass and provides an indication of changes in the overall compactness of the protein structure. Relatively stable Rg values with limited fluctuations generally indicate that the overall dimensions of the protein remain comparatively consistent during the simulation.

The three complexes showed relatively narrow Rg ranges throughout the simulation (Table 2, Figure 6, and Supplementary Figure S6). For the CZP complex, Rg values ranged from 3.521 Å at frame 315 to 3.712 Å at frame 929, corresponding to a range of 0.191 Å, with an average value of 3.618 Å. The NZP complex showed values between 3.396 Å at frame 900 and 3.583 Å at frame 222, with a range of 0.187 Å and an average of 3.496 Å. For the OXA complex, Rg values ranged from 3.462 Å at frame 223 to 3.645 Å at frame 649, corresponding to a range of 0.183 Å, with an average value of 3.551 Å.

The relatively small Rg variations observed for all three complexes indicate that the overall compactness of the simulated protein structures remained comparatively consistent throughout the trajectories. NZP showed the lowest average Rg among the three complexes, although this difference alone should not be interpreted as evidence of superior ligand stability or stronger binding. The Rg profiles remained relatively consistent after approximately 20 ns, suggesting no substantial change in the overall dimensions of the simulated protein structures during the later stages of the trajectories.

Overall, the Rg analysis indicates that all three ligand-bound isolated α1-subunit models maintained relatively stable global compactness during the simulations. However, Rg alone cannot establish ligand-induced structural effects, binding-site stability, or receptor activity.

Solvent Accessible Surface Area (SASA) Analysis

SASA was analyzed to examine changes in the solvent exposure and surface characteristics of the simulated protein–ligand complexes during the 100 ns MD simulations. SASA provides information about the surface area of a molecular system that is accessible to the surrounding solvent and can be used to monitor changes in solvent exposure and overall conformational behavior during a simulation.

The SASA profiles of the CZP, NZP, and OXA complexes are presented in Table 2, Figure 6E, and Supplementary Figure S6. The CZP complex showed SASA values ranging from 152.907 Å² at frame 293 to 508.692 Å² at frame 986, corresponding to a range of 355.785 Å², with an average value of 274.916 Å². The NZP complex exhibited values between 161.341 Å² at frame 12 and 337.338 Å² at frame 243, with a range of 175.997 Å² and an average value of 216.166 Å². For the OXA complex, SASA values ranged from 136.154 Å² at frame 223 to 485.842 Å² at frame 814, corresponding to a range of 349.688 Å², with an average value of 306.028 Å².

The lower average SASA observed for the NZP complex indicates comparatively lower solvent exposure of the analyzed molecular system during the simulation, whereas the higher average value for OXA reflects greater solvent-accessible surface area. The comparatively narrower SASA range observed for NZP also indicates less variation in solvent exposure relative to CZP and OXA. The SASA profiles became relatively consistent after approximately 25 ns, although fluctuations remained throughout the trajectories.

Overall, the SASA analysis indicates differences in solvent exposure and surface behavior among the three simulated complexes. However, SASA alone cannot establish ligand burial depth, binding affinity, complex stability, or biological efficacy. Interpretation of ligand-specific solvent exposure would require ligand SASA or protein–ligand interface SASA, together with complementary analyses such as protein–ligand contacts, hydrogen-bond occupancy, and ligand–protein distance measurements.

Hydrogen Bond Interaction Analysis

The hydrogen-bonding dynamics of the ligand–protein complexes were monitored throughout the 100 ns MD simulations to examine the persistence of polar interactions during the trajectories (Figure 6). The CZP complex maintained at least one hydrogen bond during a substantial portion of the simulation, with occasional increases to two to four hydrogen bonds. The mean hydrogen-bond count was approximately 1.11, indicating that polar contacts were maintained for a considerable portion of the trajectory [53–55].

NZP showed a more variable hydrogen-bonding pattern, with periods of hydrogen-bond formation interspersed with frames in which these contacts were absent. The complex formed a maximum of three hydrogen bonds, with an average of approximately 1.01. This pattern indicates intermittent polar contacts and greater variation in hydrogen-bond occupancy compared with the CZP complex [56].

OXA exhibited the most dynamic hydrogen-bonding profile among the three complexes. Hydrogen bonds were absent in a number of frames, while transient increases of up to five hydrogen bonds were observed in some portions of the trajectory. Despite these fluctuations, the mean hydrogen-bond count was approximately 1.11, similar to that observed for CZP [54,57]. The transient increases indicate that OXA was capable of forming multiple polar contacts during particular stages of the simulation, although these interactions were not continuously maintained.

Overall, the hydrogen-bond analysis indicates differences in the persistence and variability of polar contacts among the three ligand-bound complexes. CZP showed comparatively sustained hydrogen-bond occupancy, whereas NZP displayed greater variation in hydrogen-bond formation. OXA exhibited more pronounced fluctuations, including occasional periods with multiple simultaneous hydrogen bonds. These observations describe the dynamic polar

interaction patterns of the simulated complexes but should not be interpreted as direct measures of binding affinity or receptor activity.

Protein-ligand contact analysis

Simulation interaction diagram (SID) analysis was performed to characterize the non-covalent interaction patterns between the ligands and the isolated α1-subunit model throughout the 100 ns MD simulations. Hydrophobic interactions, ionic interactions, hydrogen bonds, and water-mediated contacts were examined to assess the persistence and distribution of protein–ligand contacts during the trajectories (Figure 7).

The CZP complex showed recurrent contacts with LYS105, LYS117, and LYS156, with reported interaction fractions of 0.04, 0.74, and 0.08, respectively (Figure 7A). Among these residues, LYS117 showed the highest reported interaction fraction, indicating that this contact was observed more frequently during the simulation. The NZP complex exhibited contacts involving HIS102, TYR160, LYS384, and THR385, with reported interaction fractions of 1.28, 1.60, 0.19, and 0.08, respectively (Figure 7B). The OXA complex displayed a broader interaction pattern involving THR13, ARG17, ASN87, LYS93, ASP98, PHE101, HIS102, SER107, ALA109, THR113, LYS117, TYR160, ALA161, GLN204, SER205, and TYR210, with reported interaction fractions ranging from 0.01 to 0.48 (Figure 7C). SER107 showed the highest reported interaction fraction among the OXA-associated residues.

Overall, the three complexes displayed distinct interaction patterns during the simulations. CZP showed recurrent contacts with a smaller subset of residues, NZP exhibited interactions involving several residues including HIS102 and TYR160, and OXA displayed a broader distribution of contacts across the simulated α1-subunit model. These differences indicate variation in the persistence and distribution of protein–ligand interactions during the trajectories. However, SID analysis describes interaction occurrence rather than directly measuring binding affinity or binding strength.

Ligand-protein contact analysis

Ligand–protein interactions contribute to the observed behavior of small molecules within a protein environment, and Simulation Interaction Diagram (SID) analysis revealed distinct interaction patterns for CZP, NZP, and OXA during the 100 ns MD simulations of the isolated α1-subunit model derived from PDB ID 6HUO. CZP showed recurrent hydrophobic contact with PHE100 and a side-chain hydrogen bond with THR99, with the latter exhibiting approximately 58% occupancy. These interactions indicate relatively persistent polar and nonpolar contacts during the simulation. NZP exhibited a hydrogen bond with HIS102 at approximately 85% occupancy, together with π–π interactions involving TYR160 at approximately 30–40% occupancy and additional hydrophobic contacts. These interactions indicate comparatively persistent polar and aromatic contacts during the trajectory. OXA displayed a broader but more variable interaction pattern, involving predominantly hydrophobic contacts and intermittent hydrogen bonding associated with its hydroxyl group. Overall, the three ligands exhibited distinct patterns in the type and persistence of protein–ligand contacts. The observed differences may reflect the influence of ligand structure, polarity, and aromatic features on their interaction patterns within the simulated α1-subunit environment.

Biological Activities Using PASS

PASS analysis was performed to explore the predicted biological activity profiles of the selected BZDs. Predicted activities were interpreted according to their probability of activity (Pa), with Pa > 0.7 considered a higher predicted probability, 0.5–0.7 considered an intermediate predicted probability, and Pa < 0.5 considered a lower predicted probability [58]. The analyzed compounds—CDP, chlorazepate, CBZ, clonazepam, ESZ, FZP, MDZ, NZP, OXA, and TMZ—showed diverse predicted biological activities, including muscle relaxant, anticonvulsant, anxiolytic, GABA receptor-related, and antiepileptic activities.

Antineurotic activity was predicted with Pa > 0.7 for chlorazepate, ESZ, FZP, and MDZ. Muscle relaxant activity showed lower predicted probabilities for CDP, ESZ, and CBZ. Anticonvulsant activity showed Pa > 0.7 for most compounds, with CDP representing an exception. Higher predicted probabilities for anxiolytic activity were observed for MDZ, FZP, ESZ, TMZ, and OXA. GABA receptor agonist activity was also predicted with Pa > 0.7 for OXA, TMZ, ESZ, FZP, and MDZ. Similarly, OXA, ESZ, FZP, and MDZ showed higher predicted probabilities for antiepileptic activity. FZP, clonazepam, and OXA were additionally predicted to have CYP3A4 substrate activity with relatively high Pa values.

The predicted biological activities are summarized in Table 3. Overall, the PASS results indicate that the selected BZDs share several predicted CNS-related activity profiles, while differences in Pa values were observed among individual compounds. These predictions provide computational indications of possible biological activities but do not establish experimental efficacy, receptor agonism, or clinical pharmacological effects.

Comparative ADMET Analysis of BZDs

The predicted ADMET profiles of the ten BZDs showed variation in absorption, permeability, metabolic interactions, and toxicity-related parameters. The compounds showed predicted human intestinal absorption (HIA) values ranging from 0.929 to 1.000, together with predicted Caco-2 permeability values ranging from 0.500 to 0.887, indicating potentially favorable intestinal absorption and cellular permeability characteristics [59]. Predicted blood–brain barrier (BBB) values ranged from 0.837 to 0.991, suggesting the potential for CNS access [60]. These computational predictions are consistent with the CNS-directed use of several BZDs but should not be interpreted as direct measures of clinical efficacy or confirmed BBB penetration.

Differences were also observed in the predicted CYP450 interaction profiles. OXA, TMZ, CDP, and NZP were predicted to be non-inhibitors of both CYP3A4 and CYP2C9, whereas CLZ, ESZ, CBZ, and FZP showed predicted CYP3A4 inhibitory activity. CZP and NZP were

predicted to inhibit CYP3A4, while ESZ, CBZ, CZP, NZP, and MDZ showed predicted CYP2C9 inhibitory activity. These results indicate potential differences in CYP-mediated metabolic interactions among the compounds. However, enzyme inhibition predictions alone cannot establish actual metabolic clearance, plasma accumulation, or the duration of pharmacological effects in vivo.

Toxicity-related predictions also varied among the compounds. The predicted carcinogenicity scores ranged from 0.642 to 0.809, while high predicted *Tetrahymena pyriformis* toxicity (hTPT) was observed across the series. Acute oral toxicity predictions placed most compounds within Categories III–IV, whereas MDZ was assigned to Category II in the applied prediction model [61]. These computational toxicity classifications should be interpreted as model-based predictions rather than direct evidence of clinical safety or toxicity.

Overall, the ADMET analysis revealed compound-dependent differences in predicted absorption, permeability, CYP450 interactions, and toxicity-related parameters. These findings provide a comparative computational assessment of the selected BZDs and may help identify differences in their predicted pharmacokinetic and toxicological profiles. Experimental pharmacokinetic, metabolic, and toxicological studies would be required to confirm these predictions.

Discussion

The present study combined DFT, molecular docking, MD simulation, PASS prediction, and ADMET profiling to examine the structural, electronic, and predicted pharmacokinetic properties of selected BZDs in relation to an isolated α1-subunit model derived from the human GABA-A receptor structure (PDB ID: 6HUO). The analyses revealed differences among the compounds in their electronic descriptors, predicted docking poses, conformational behaviour, and computationally predicted pharmacological and pharmacokinetic properties. Together,

these methods provide complementary perspectives on molecular characteristics and predicted ligand-associated behaviour. The docking and MD findings, however, should be interpreted within the context of the isolated α1-subunit model rather than as direct evidence of binding at the canonical benzodiazepine-binding site, receptor modulation, or experimental pharmacological activity.

FMO analysis revealed differences in the HOMO–LUMO energy gaps of the investigated compounds, providing insight into their predicted electronic reactivity and related molecular properties. CDP exhibited the lowest HOMO–LUMO gap, suggesting comparatively greater electronic reactivity, whereas CBZ had the highest gap, indicating comparatively lower electronic reactivity and greater resistance to electronic perturbation within the applied framework. These observations relate to the concepts of chemical hardness and softness, whereby softer molecules generally exhibit greater electronic polarizability and responsiveness to changes in their electronic environment [56]. NZP showed the highest calculated softness among the studied compounds, suggesting comparatively greater electronic polarizability. Although these descriptors help distinguish the electronic characteristics of the BZDs, they do not independently demonstrate improved receptor accommodation, binding affinity, or biological activity.

The electronic analysis was complemented by thermodynamic and electrostatic calculations. FZP showed the most negative calculated total energy among the investigated compounds. However, total energies calculated for individual molecules should not be interpreted directly as measures of their stability relative to one another or of their receptor-binding strength without appropriate comparative calculations. Dipole moment analysis identified ESZ as having the highest calculated dipole moment, indicating comparatively greater molecular polarity and a different charge distribution that may influence intermolecular interactions. Molecular electrostatic potential (MEP) mapping also revealed regions of relatively negative

and positive electrostatic potential in compounds such as NZP, CLZ, and CZP [36]. Negative electrostatic regions, particularly around oxygen atoms, may serve as potential sites for interactions with suitable partners, while positive regions may interact with electron-rich sites. These calculations help characterize molecular polarity and potential interaction regions but do not establish receptor-binding specificity or pharmacological activity.

Molecular docking revealed differences in the predicted poses and docking scores of the investigated BZDs within the selected region of the isolated α1-subunit model. OXA produced a docking score of −7.3 kcal/mol, close to that of the co-crystallized ligand alprazolam (ALP), which scored −7.5 kcal/mol. The hydroxyl group at C3 of OXA may contribute to the predicted hydrogen-bonding interactions with residues such as SER205 and THR207. NZP also showed a comparatively favourable docking score, potentially reflecting contributions from its C7 nitro substituent to polarity and electrostatic interactions. TYR210, TYR160, and PHE100 participated in various predicted aromatic or hydrophobic contacts across the docked compounds. These results suggest that hydrogen bonding, aromatic contacts, and hydrophobic interactions may contribute to the predicted poses within the selected α1-subunit region. Nevertheless, docking scores and predicted contacts are dependent on the model and scoring function used. Because the α1–γ2 interface was not retained in the model, these findings do not establish binding at the canonical benzodiazepine-binding site or demonstrate receptor modulation.

From a structure–activity relationship (SAR) perspective, substitutions at N1, C3, C5, and C7 may influence the physicochemical properties and predicted interaction patterns of BZDs. The differences observed in docking scores may reflect the combined effects of hydrogen-bonding capacity, polarity, aromatic character, and steric features on ligand positioning within the selected α1-subunit region. For example, the C3 hydroxyl group of OXA may contribute to its predicted hydrogen-bonding pattern, whereas the C7 nitro group of NZP may influence its local

electrostatic environment. Differences in ring geometry and substituent size among compounds such as FZP and CBZ may also contribute to their predicted docking behaviour. These interpretations remain in computational associations rather than experimentally established SAR relationships. The present results therefore do not establish that specific substitutions increase or decrease receptor affinity. Further structural and experimental studies would be needed to clarify how these molecular features influence interactions with the complete GABA-A receptor.

To examine the conformational behaviour of selected ligand–protein complexes, 100 ns MD simulations were performed for CZP, NZP, and OXA. Analysis of protein RMSD, ligand RMSD, radius of gyration (Rg), and solvent-accessible surface area (SASA) revealed differences among the three simulated systems. NZP showed the lowest average protein and ligand RMSD, together with relatively consistent compactness and solvent-exposure profiles during the simulation. These observations indicate comparatively lower conformational deviation in the NZP-associated system over the simulated period. In contrast, OXA exhibited substantial ligand RMSD fluctuations during the later stages of the trajectory, indicating changes in its position or conformation relative to the initial reference structure. This contrast between OXA's initial docking score and its subsequent RMSD behaviour illustrates the different information provided by docking and MD simulation: docking estimates the favourability of a predicted pose using a scoring function, whereas MD follows structural changes over time under the simulated conditions. However, RMSD, Rg, and SASA alone cannot establish ligand retention, binding affinity, or receptor activity. The observed differences should therefore be interpreted as trajectory-dependent behaviour within the simulated systems.

Hydrogen-bond occupancy and SID analyses further highlighted differences in the predicted interaction patterns of NZP, OXA, and CZP. NZP showed relatively persistent hydrogen-

bonding and aromatic interactions involving residues such as HIS102 and TYR160 during portions of the trajectory. OXA formed multiple hydrogen bonds at certain stages, although these interactions varied over time. CZP displayed both polar and hydrophobic contacts, including recurrent interactions involving PHE100 and THR99. The recurrence of residues such as HIS102, TYR160, SER205, and PHE100 across the analyses indicates that they contributed to predicted interactions within the simulated isolated α1-subunit environment. Nevertheless, the frequency or persistence of individual contacts does not independently establish binding affinity, binding specificity, or receptor function. These observations describe interactions within the selected structural model and should not be taken as definitive evidence of interactions at the canonical α1–γ2 benzodiazepine-binding interface.

PASS and ADMET analyses provided additional predictions regarding the potential biological activities and pharmacokinetic characteristics of the selected BZDs. PASS predicted several CNS-related activities, including anxiolytic, anticonvulsant, muscle relaxant, and GABA receptor-related activities, with differences in Pa values among the compounds. Higher predicted probabilities for several anxiolytic and GABA receptor-related activities were observed for OXA, ESZ, FZP, MDZ, and TMZ. The ADMET analysis also predicted intestinal absorption, Caco-2 permeability, and blood–brain barrier (BBB) permeability across the investigated compounds, suggesting potentially favourable absorption characteristics and possible CNS exposure according to the applied prediction models. These results do not, however, establish oral bioavailability or actual BBB penetration, which depend on multiple physicochemical, biological, and pharmacokinetic factors.

Differences were also observed in the predicted CYP450 interaction profiles. OXA, TMZ, and CDP were predicted to be non-inhibitors of both CYP3A4 and CYP2C9. In contrast, CLZ, CBZ, CZP, NZP, and FZP were predicted to inhibit CYP3A4, while ESZ, CZP, and MDZ were predicted to inhibit CYP2C9. These profiles suggest potential differences in the compounds'

predicted metabolic interaction characteristics. However, computational enzyme-inhibition predictions alone cannot establish changes in drug metabolism, systemic accumulation, drug exposure, or clinical safety. The predicted toxicity parameters should likewise be treated as model-based estimates rather than direct evidence of toxicity or safety. Experimental testing would be required to determine whether these predicted properties translate into measurable biological or clinical effects.

Several limitations should be considered when interpreting these findings. The docking and MD simulations used the isolated GABA-A receptor α1 subunit (Chain D), allowing the structural and ligand-associated properties of this subunit to be examined without modelling the complete receptor. Consequently, the predicted interactions are specific to the selected structural model and do not establish binding at the canonical benzodiazepine-binding interface. The substantial ligand RMSD fluctuations observed for OXA and CZP also require further examination. Inspection of the trajectories and verification of the RMSD calculations would help determine whether these changes reflect ligand displacement, conformational variation, or methodological factors. In addition, the selected complexes were analysed using single MD trajectories, leaving the reproducibility of their observed behaviour across independent simulations undetermined. The DFT descriptors, docking scores, PASS predictions, and ADMET profiles provide computational estimates rather than experimental confirmation of binding affinity, pharmacological activity, pharmacokinetic behaviour, or clinical safety and efficacy. No experimental validation was performed in the present study. Independent MD simulations, detailed trajectory analysis, and appropriate biochemical and pharmacological experiments would help assess the robustness of these observations and clarify their biological relevance.

Overall, the investigated BZDs displayed distinct electronic, docking, dynamic, and predicted ADMET profiles. NZP showed comparatively lower conformational deviation during the MD

simulation and relatively persistent predicted interaction patterns, whereas OXA had a favourable initial docking score but exhibited greater ligand RMSD fluctuations during the later stages of the trajectory. These contrasting observations illustrate the value of combining electronic-structure calculations, docking, MD simulation, PASS prediction, and ADMET profiling to compare molecular properties and predicted behaviour. The findings remain computational and should be interpreted in the context of the isolated α1-subunit model and the limitations of the prediction methods. Further studies using independent MD trajectories, the complete receptor system where appropriate, and experimental assays are needed to establish the relevance of the predicted interactions and assess their potential pharmacological significance.

Conclusion

This study integrated DFT, molecular docking, MD simulations, PASS prediction, and ADMET profiling to comparatively characterize ten BZDs. The compounds exhibited distinct electronic properties, predicted binding interactions, conformational behaviors, and computationally predicted biological activity and pharmacokinetic profiles. Among the investigated compounds, OXA showed the most favorable docking score, whereas NZP exhibited comparatively lower ligand RMSD during the 100-ns MD simulation. However, the substantial ligand RMSD fluctuations observed for OXA and CZP warrant further trajectory inspection.

These findings provide a comparative computational assessment of BZD properties and may inform future investigations. Nevertheless, because docking and MD simulations used an isolated GABA-A receptor α1 subunit rather than the complete receptor, the results do not establish binding at the canonical benzodiazepine-binding interface or demonstrate receptor modulation. Similarly, PASS and ADMET outputs represent computational predictions rather

738 than experimental evidence of pharmacological activity, safety, or clinical efficacy. Further
739 studies using the complete receptor structure, independent MD simulations, and experimental
740 validation are needed to establish the biological relevance of these findings.
741
742 **References**

743 1. Lorenz-Guertin, J. M. *et al.* Inhibitory and excitatory synaptic neuroadaptations in the
744 diazepam tolerant brain. *Neurobiol. Dis.* **185**, (2023).
745 2. Chang, Y., Xie, X., Liu, Y., Liu, M. & Zhang, H. Exploring clinical applications and
746 long-term effectiveness of benzodiazepines: An integrated perspective on mechanisms,
747 imaging, and personalized medicine. *Biomed. Pharmacother.* **173**, 116329–116329
748 (2024).
749 3. Goldschen-Ohm, M. P. Benzodiazepine Modulation of GABAA Receptors: A
750 Mechanistic Perspective. *Biomolecules* **12**, (2022).
751 4. Zhu, S. *et al.* Structural and dynamic mechanisms of GABAA receptor modulators with
752 opposing activities. *Nat. Commun.* **13**, (2022).
753 5. Tafet, G. E. & Nemeroff, C. B. Pharmacological Treatment of Anxiety Disorders: The
754 Role of the HPA Axis. *Front. Psychiatry* **11**, (2020).
755 6. Maramai, S., Benchekroun, M., Ward, S. E. & Atack, J. R. Subtype Selective γ-
756 Aminobutyric Acid Type A Receptor (GABAAR) Modulators Acting at the
757 Benzodiazepine Binding Site: An Update. *J. Med. Chem.* **63**, 3425–3446 (2020).
758 7. Ghit, A., Assal, D., Al-Shami, A. S. & Hussein, D. E. E. GABAA receptors: structure,
759 function, pharmacology, and related disorders. *Journal of Genetic Engineering and*
760 *Biotechnology* **19**, (2021).
761 8. Sigel, E. & Steinmann, M. E. Structure, Function, and Modulation of GABAA
762 Receptors. *J. Biol. Chem.* **287**, 40224 (2012).

9. Wen, Y. *et al.* Glutamate and GABAA receptor crosstalk mediates homeostatic regulation of neuronal excitation in the mammalian brain. *Signal Transduct. Target. Ther.* **7**, (2022).

10. Markota, M., Rummans, T. A., Bostwick, J. M. & Lapid, M. I. Benzodiazepine Use in Older Adults: Dangers, Management, and Alternative Therapies. *Mayo Clin. Proc.* **91**, 1632–1639 (2016).

11. Edinoff, A. N. *et al.* Benzodiazepines: Uses, dangers, and clinical considerations. *Neurol. Int.* **13**, 594–607 (2021).

12. Adverse effects of benzodiazepines. *The Lancet* **335**, 1584 (1990).

13. Hähnke, V. D., Kim, S. & Bolton, E. E. PubChem chemical structure standardization. *J. Cheminform.* **10**, 1–40 (2018).

14. Allouche, A. R. Gabedita - A graphical user interface for computational chemistry softwares. *J. Comput. Chem.* **32**, 174–182 (2011).

15. Frisch, M. J. *et al.* Gaussian 16 Revision C.01. Preprint at https://gaussian.com (2016).

16. Geerlings, P., De Proft, F. & Langenaeker, W. Conceptual density functional theory. *Chem. Rev.* **103**, 1793–1873 (2003).

17. Uzzaman, M., Ahsan, A. & Uddin, M. N. Comparative assessment of some benzodiazepine drugs based on Density Functional Theory, molecular docking, and ADMET studies. *European Journal of Chemistry* **12**, 412–418 (2021).

18. Masiulis, S. *et al.* CryoEM structure of human full-length heteromeric alpha1beta3gamma2L GABA(A)R in complex with alprazolam (Xanax), GABA and megabody Mb38. *Worldwide Protein Data Bank* https://doi.org/10.2210/PDB6HUO/PDB (2019) doi:10.2210/PDB6HUO/PDB.

19. Biovia, D. S. Discovery studio visualizer. *San Diego, CA, USA* **936**, 240–249 (2017).

20. Baroroh, S.Si., M.Biotek., U., Muscifa, Z. S., Destiarani, W., Rohmatullah, F. G. & Yusuf, M. Molecular interaction analysis and visualization of protein-ligand docking using Biovia Discovery Studio Visualizer. *Indonesian Journal of Computational Biology (IJCB)* **2**, 22–30 (2023).

21. Guex, N. & Peitsch, M. C. SWISS-MODEL and the Swiss-PdbViewer: An environment for comparative protein modeling. *Electrophoresis* **18**, 2714–2723 (1997).

22. Ramírez, D. & Caballero, J. Is It Reliable to Take the Molecular Docking Top Scoring Position as the Best Solution without Considering Available Structural Data? *Molecules 2018, Vol. 23, Page 1038* **23**, 1038 (2018).

23. Trott, O. & Olson, A. J. AutoDock Vina: Improving the speed and accuracy of docking with a new scoring function, efficient optimization, and multithreading. *J. Comput. Chem.* **31**, 455–461 (2010).

24. El-Malah, A. A. *et al.* Design, synthesis, molecular docking, and molecular dynamic studies of novel quinazoline derivatives as phosphodiesterase 7 inhibitors. *Front. Pharmacol.* **15**, (2024).

25. Klíma, M., Celný, D., Janek, J. & Kolafa, J. Properties of water and argon clusters developed in supersonic expansions. *Journal of Chemical Physics* **159**, (2023).

26. Roy, S. *et al.* CLICK-chemoproteomics and molecular dynamics simulation reveals pregnenolone targets and their binding conformations in Th2 cells. *Front. Immunol.* **14**, (2023).

27. Cheng, F. *et al.* admetSAR: a comprehensive source and free tool for assessment of chemical ADMET properties. Preprint at (2012).

28. Filimonov, D. A. *et al.* Prediction of the biological activity spectra of organic compounds using the PASS online web resource. *Chem. Heterocycl. Compd. (N. Y).* **50**, 444–457 (2014).

812 29. Geerlings, P., De Proft, F. & Langenaeker, W. Conceptual Density Functional Theory.
813 *Chem. Rev.* **103**, 1793–1874 (2003).
814 30. Garbett, N. C. & Chaires, J. B. Thermodynamic studies for drug design and screening.
815 *Expert Opin. Drug Discov.* **7**, 299–314 (2012).
816 31. Lien, E., Guo, Z., Li, R., sciences, C. S.-J. of pharmaceutical & 1982, undefined. Use of
817 dipole moment as a parameter in drug–receptor interaction and quantitative structure–
818 activity relationship studies. *ElsevierEJ Lien, ZR Guo, RL Li, CT SuJournal of*
819 *pharmaceutical sciences, 1982•Elsevier*
820 https://www.sciencedirect.com/science/article/pii/S0022354915442224.
821 32. Morad, R., Akbari, M. & Maaza, M. Theoretical study of chemical reactivity descriptors
822 of some repurposed drugs for COVID-19. *MRS Adv.* **8**, 656–660 (2023).
823 33. Miar, M., Shiroudi, A., Pourshamsian, K., Oliaey, A. R. & Hatamjafari, F. DFT study
824 and NBO analysis of solvation/substituent effects of 3-phenylbenzo[d]thiazole-2(3H)-
825 imine derivatives. *Journal of the Serbian Chemical Society* **85**, 1445–1462 (2020).
826 34. Gould, T., Hashimi, Z., Kronik, L. & Dale, S. Single excitation energies obtained from
827 the ensemble HOMO-LUMO gap: exact results and approximations.
828 https://doi.org/10.26434/CHEMRXIV-2022-786FK (2022)
829 doi:10.26434/CHEMRXIV-2022-786FK.
830 35. Aihara, J. I. Reduced HOMO-LUMO Gap as an Index of Kinetic Stability for Polycyclic
831 Aromatic Hydrocarbons. *Journal of Physical Chemistry A* **103**, 7487–7495 (1999).
832 36. Bayoumy, A. M., Ibrahim, M. & Omar, A. Mapping molecular electrostatic potential
833 (MESP) for fulleropyrrolidine and its derivatives. *Opt. Quantum Electron.* **52**, (2020).
834 37. Gadre, S. R., Suresh, C. H. & Mohan, N. Electrostatic potential topology for probing
835 molecular structure, bonding and reactivity. *Molecules* **26**, (2021).

836 38. Roy, M. S., Sarkar, B. K. & Kundu, S. K. Site specific binding pattern of
837 benzodiazepines with GABAA receptor and related impact on their activities in the
838 human body: An in silico method based study. *Heliyon* **10**, (2024).
839 39. Thakur, M., Thakur, A. & Gotmare, S. DOCKING STUDIES OF
840 BENZODIAZEPINES AS A POSITIVE ALLOSTERIC MODULATOR OF GABA-A
841 RECEPTOR. *International Journal of Research and Development in Pharmacy & Life*
842 *Sciences* **4**, 1577–1581 (2015).
843 40. Elgarf, A. A. *et al.* Different benzodiazepines bind with distinct binding modes to
844 GABAA receptors. *ACS Chem. Biol.* **13**, 2033–2039 (2018).
845 41. Phulera, S. *et al.* Cryo-EM structure of the benzodiazepine-sensitive α1β1γ2S tri-
846 heteromeric GABAA receptor in complex with GABA. *Elife* **7**, e39383 (2018).
847 42. Campo-Soria, C., Chang, Y. & Weiss, D. S. Mechanism of action of benzodiazepines
848 on GABAA receptors. *Br. J. Pharmacol.* **148**, 984–990 (2006).
849 43. Borea, P. A., Hamor, T. A. & Martin, I. L. Structure-Activity Relationships at the
850 Benzodiazepine Receptor. *Analysis of Psychiatric Drugs* 473–532 (2003)
851 doi:10.1385/0-89603-121-7:473.
852 44. Thakur, M., Ojha, L., Thakur, A. & Solanki, B. K. Study of active site and SAR of some
853 benzodiazepines. *J. Comput. Biol. Bioinform. Res.* **2**, 10–19 (2010).
854 45. Çınaroğlu, S. S. & Biggin, P. C. The role of loop dynamics in the prediction of ligand–
855 protein binding enthalpy. *Chem. Sci.* **14**, 6792–6805 (2023).
856 46. Williams, J. K. *et al.* Molecular dynamics analysis of a flexible loop at the binding
857 interface of the SARS-CoV-2 spike protein receptor-binding domain. *Proteins* **90**,
858 1044–1053 (2022).
859 47. Lindorff-Larsen, K., Piana, S., Dror, R. O. & Shaw, D. E. How fast-folding proteins
860 fold. *Science (1979).* **334**, 517–520 (2011).

48. Grant, B. J., Rodrigues, A. P. C., ElSawy, K. M., McCammon, J. A. & Caves, L. S. D. Bio3d: an R package for the comparative analysis of protein structures. *Bioinformatics* **22**, 2695–2696 (2006).

49. Shukla, R. & Tripathi, T. Molecular dynamics simulation of protein and protein–ligand complexes. in *Computer-aided drug design* 133–161 (Springer, 2020).

50. Vilar, S., Cozza, G. & Moro, S. Medicinal chemistry and the molecular operating environment (MOE): application of QSAR and molecular docking to drug discovery. *Curr. Top. Med. Chem.* **8**, 1555–1572 (2008).

51. Shan, Y. *et al.* How does a drug molecule find its target binding site? *J. Am. Chem. Soc.* **133**, 9181–9183 (2011).

52. Henzler-Wildman, K. & Kern, D. Dynamic personalities of proteins. *Nature* **450**, 964–972 (2007).

53. Kumari, R., Kumar, R., Consortium, O. S. D. D. & Lynn, A. g_mmpbsa□ A GROMACS tool for high-throughput MM-PBSA calculations. *J. Chem. Inf. Model.* **54**, 1951–1962 (2014).

54. Hollingsworth, S. A. & Dror, R. O. Molecular dynamics simulation for all. *Neuron* **99**, 1129–1143 (2018).

55. Yekeen, A. A., Durojaye, O. A., Idris, M. O., Muritala, H. F. & Arise, R. O. CHAPERONg: A tool for automated GROMACS-based molecular dynamics simulations and trajectory analyses. *Comput. Struct. Biotechnol. J.* **21**, 4849–4858 (2023).

56. Abraham, M. J. *et al.* GROMACS: High performance molecular simulations through multi-level parallelism from laptops to supercomputers. *SoftwareX* **1**, 19–25 (2015).

884 57. Lemkul, J. A. From Proteins to Perturbed Hamiltonians: A Suite of Tutorials for the
885 GROMACS-2018 Molecular Simulation Package [Article v1.0]. *Living J. Comput. Mol.*
886 *Sci.* **1**, 5068–5068 (2019).
887 58. Goel, R. K., Singh, D., Lagunin, A. & Poroikov, V. PASS-assisted exploration of new
888 therapeutic potential of natural products. *Medicinal Chemistry Research* **20**, 1509–1514
889 (2011).
890 59. Artursson, P., Palm, K. & Luthman, K. Caco-2 monolayers in experimental and
891 theoretical predictions of drug transport. *Adv. Drug Deliv. Rev.* **46**, 27–43 (2001).
892 60. Pajouhesh, H. & Lenz, G. R. Medicinal chemical properties of successful central
893 nervous system drugs. *NeuroRX 2005 2:4* **2**, 541–553 (2005).
894 61. Mielke, H., Strickland, J., Jacobs, M. N. & Mehta, J. M. Biometrical evaluation of the
895 performance of the revised OECD Test Guideline 402 for assessing acute dermal
896 toxicity. *Regulatory Toxicology and Pharmacology* **89**, 26–39 (2017).
897

898 Acknowledgements

899 Not applicable.

900 Declaration of Generative AI and AI-Assisted Technologies

901 During the preparation of this work, the authors used QuillBot to assist with paraphrasing and
902 language refinement to improve clarity and readability. All content generated or modified using
903 this tool was carefully reviewed and edited by the authors, who take full responsibility for the
904 integrity, accuracy, and originality of the published work.

905

906

Author contributions

Moshiur Rahman: Conceptualization, Data curation, Formal analysis, Investigation, Software, Methodology, Resources, Writing—original draft, Supervision, Visualization, Writing—review and editing. Md.Tarikul Islam: Data curation, Formal analysis, Software, Methodology, Writing—original draft, Visualization, Writing—review and editing. Shohanul Islam Sarker: Data curation, Formal analysis, Methodology, Writing—original draft, Visualization. Shamim Ahammad: Data curation, Formal analysis, Methodology, Writing—original draft, Visualization. Abir Hossen Tanvir: Data curation, Formal analysis, Methodology, Writing—original draft, Visualization. Pronob Das: Data curation, Software, Methodology, Writing—original draft.

Ethical Statement

This study is entirely computational and involved no humans, animals, or personal data, and was conducted following institutional and international ethical standards.

Data Availability Statement

All data generated or analyzed during this study are described in the published article. The computational outputs supporting the findings, including docking results, selected protein–ligand complex structures, DFT-optimized structures, ADMET predictions, and MD analysis outputs, are available from the corresponding author upon reasonable request, subject to applicable software licensing restrictions.

Additional Information

Competing Interests: The authors declare no competing interests.

Funding

The author(s) did not receive any financial support for the research, authorship, or publication of this article.

Figures

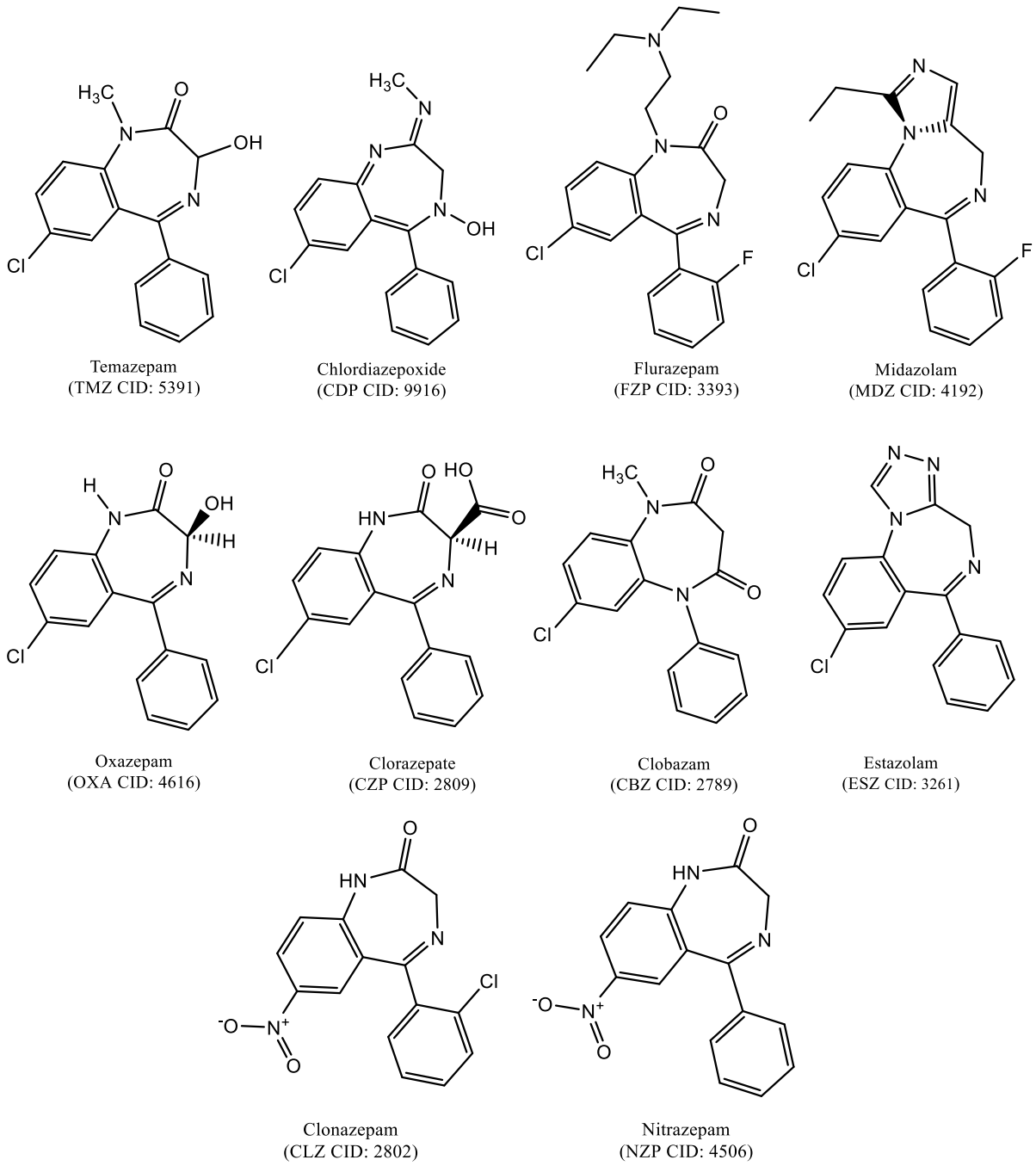


Figure 1. Chemical structures of the selected BZDs, showing their abbreviations and corresponding PubChem Compound Identifiers (CIDs).

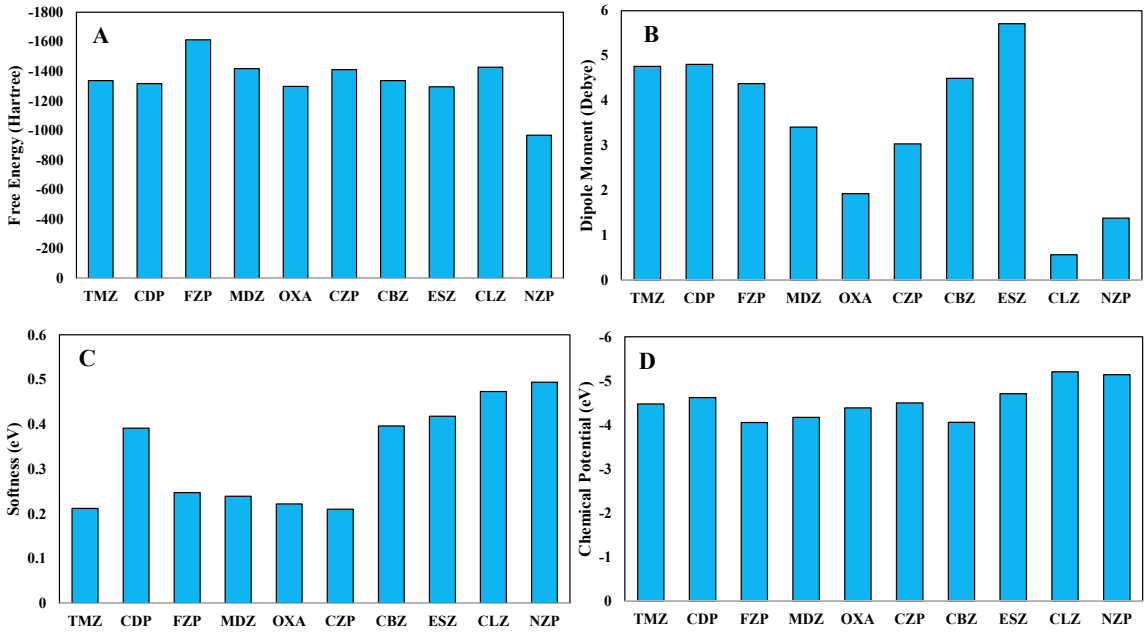
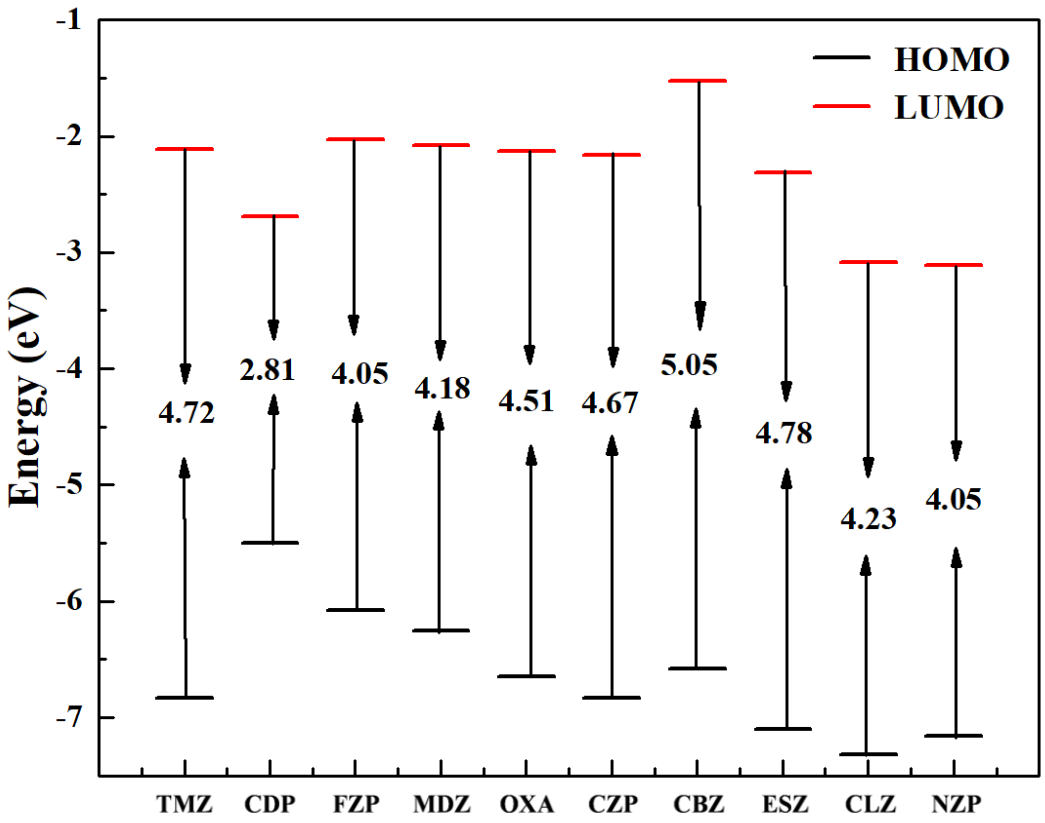


Figure 2. Comparison of calculated physicochemical and electronic descriptors of the selected BZDs: (A) Gibbs free energy, (B) dipole moment, (C) chemical softness, and (D) chemical potential.

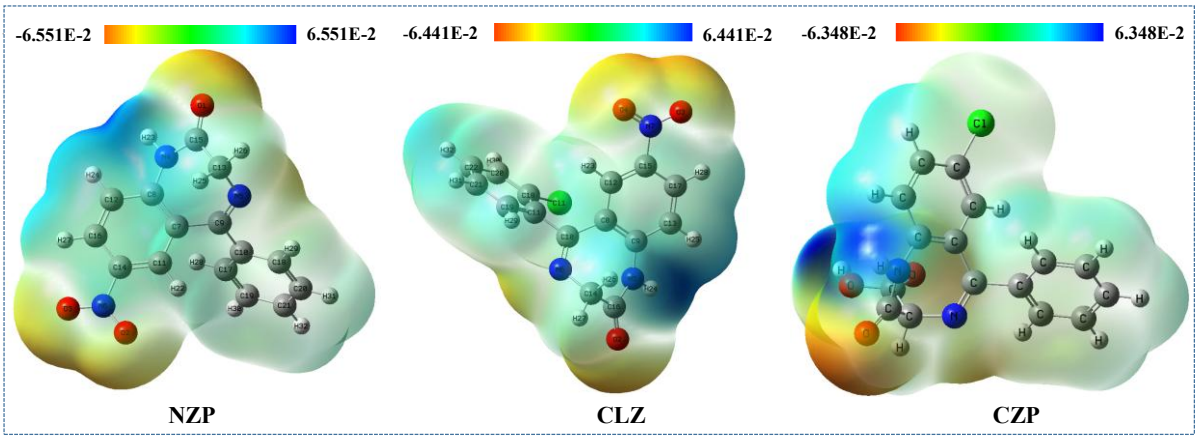


959

960 **Figure 3:** Comparison of calculated highest occupied molecular orbital–lowest unoccupied

961 molecular orbital (HOMO–LUMO) energy gaps among the selected BZDs.

962



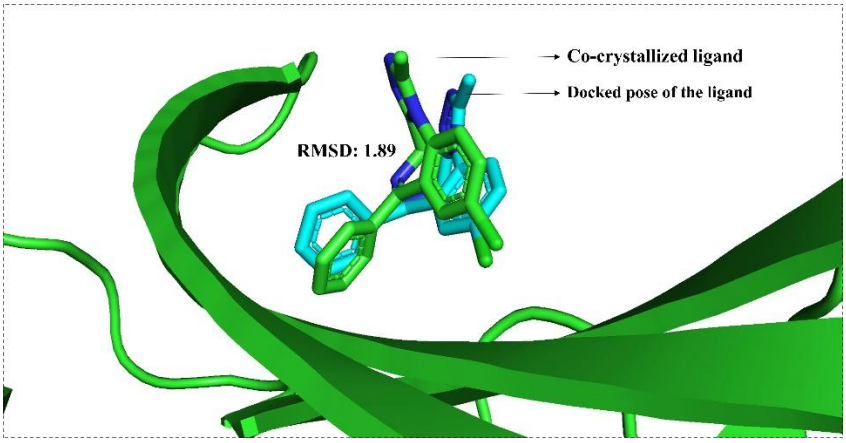
963

964 **Figure 4.** Molecular electrostatic potential (MEP) maps of the three prioritized

965 benzodiazepines, illustrating the spatial distribution of electrostatic potential across their

966 molecular surfaces.

967



968 **Figure 5:** Validation of the molecular docking protocol by superimposing the redocked ligand

969 pose onto its co-crystallized conformation.

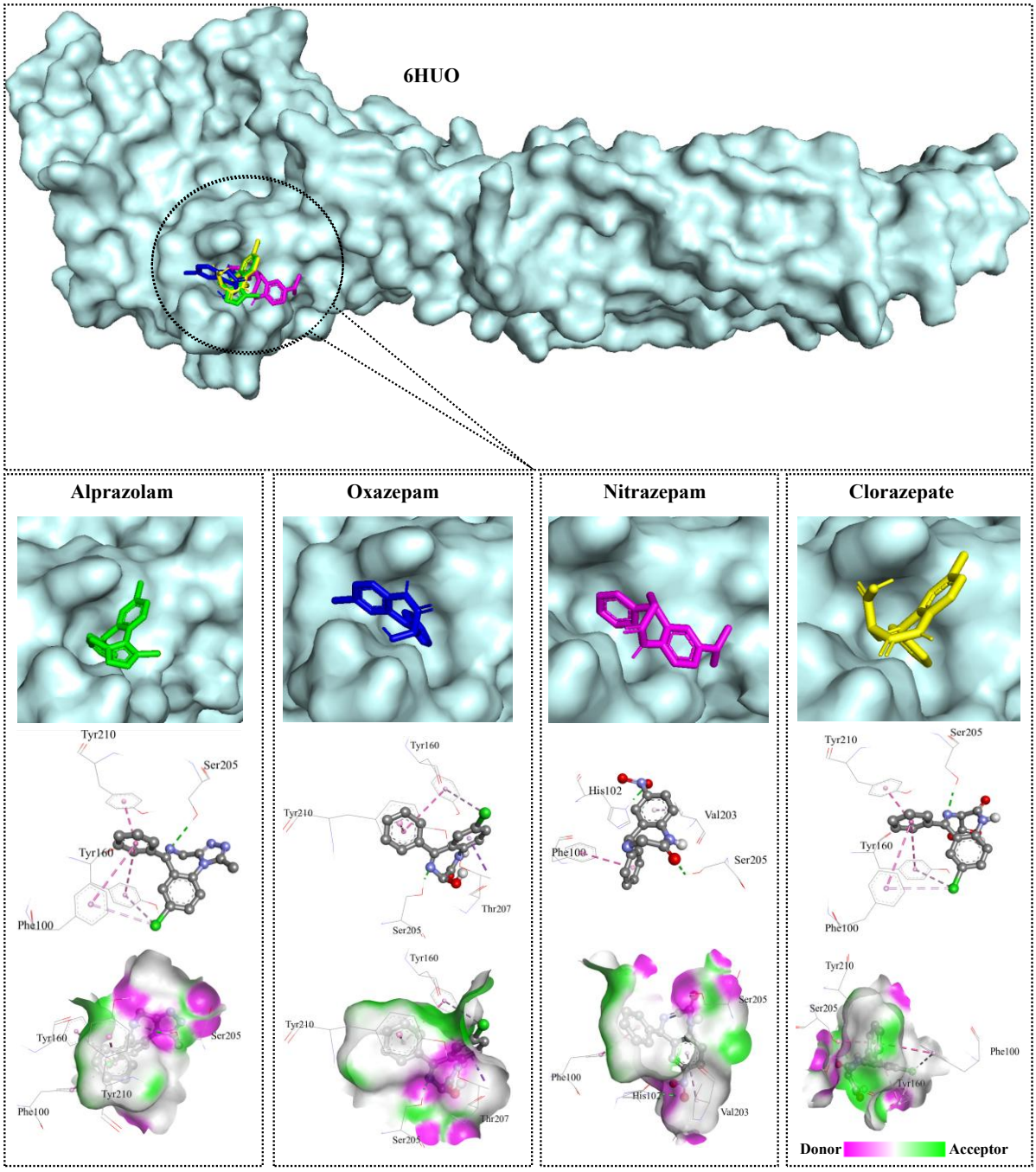
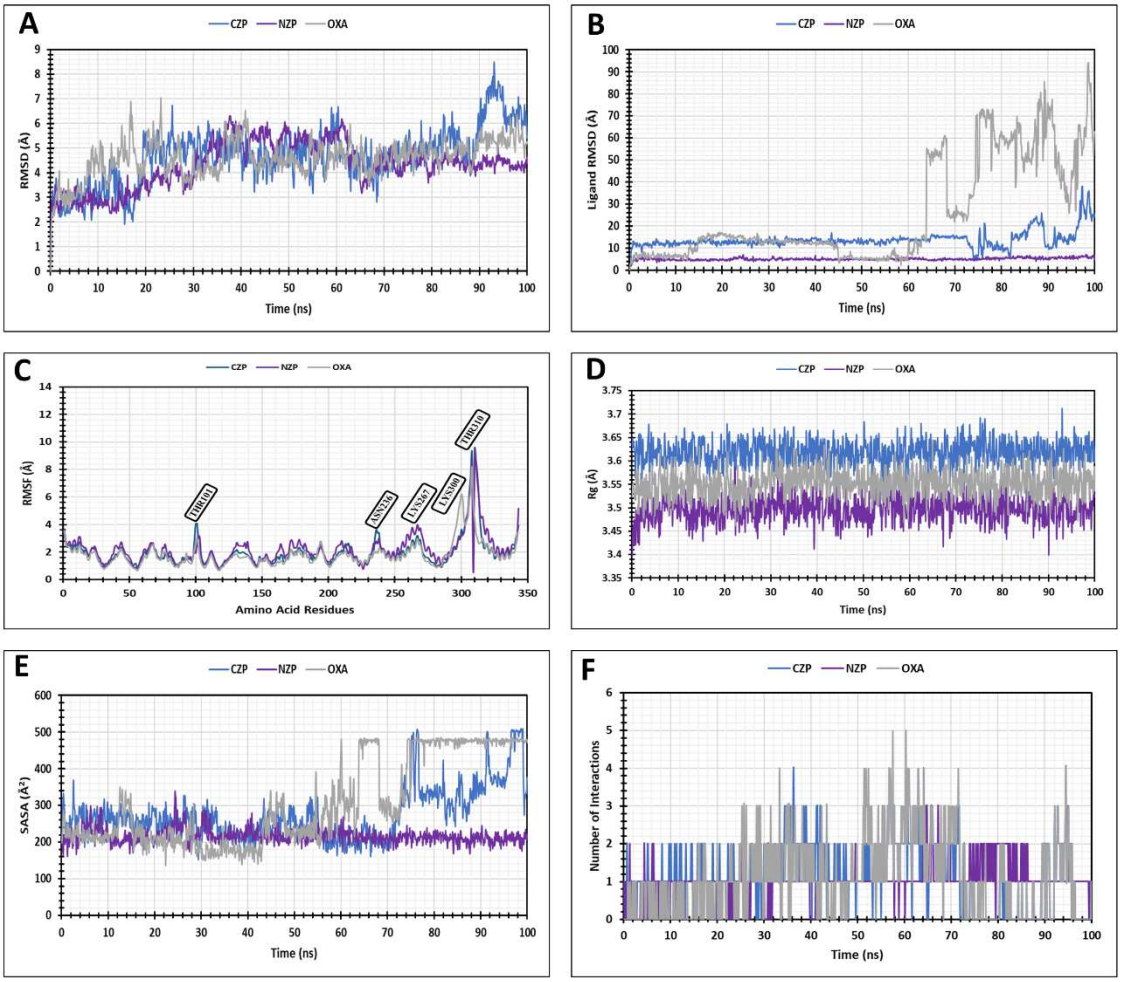


Figure 6. Comparison of the binding-site environment, non-bonded interactions, and hydrogen-bonding surfaces of the three prioritized BZDs and the co-crystallized reference ligand alprazolam (ALP) within the GABA-A receptor structure (PDB ID: 6HUO).



975 .

976 **Figure 7.** MD analysis of three prioritized BZDs docked to the isolated α1 subunit (Chain D)
977 of the GABA-A receptor (PDB ID: 6HUO) over 100 ns: (A) protein Cα RMSD, (B) ligand
978 RMSD, (C) protein Cα RMSF, (D) radius of gyration (Rg), (E) solvent-accessible surface area
979 (SASA), and (F) intermolecular hydrogen bonds.

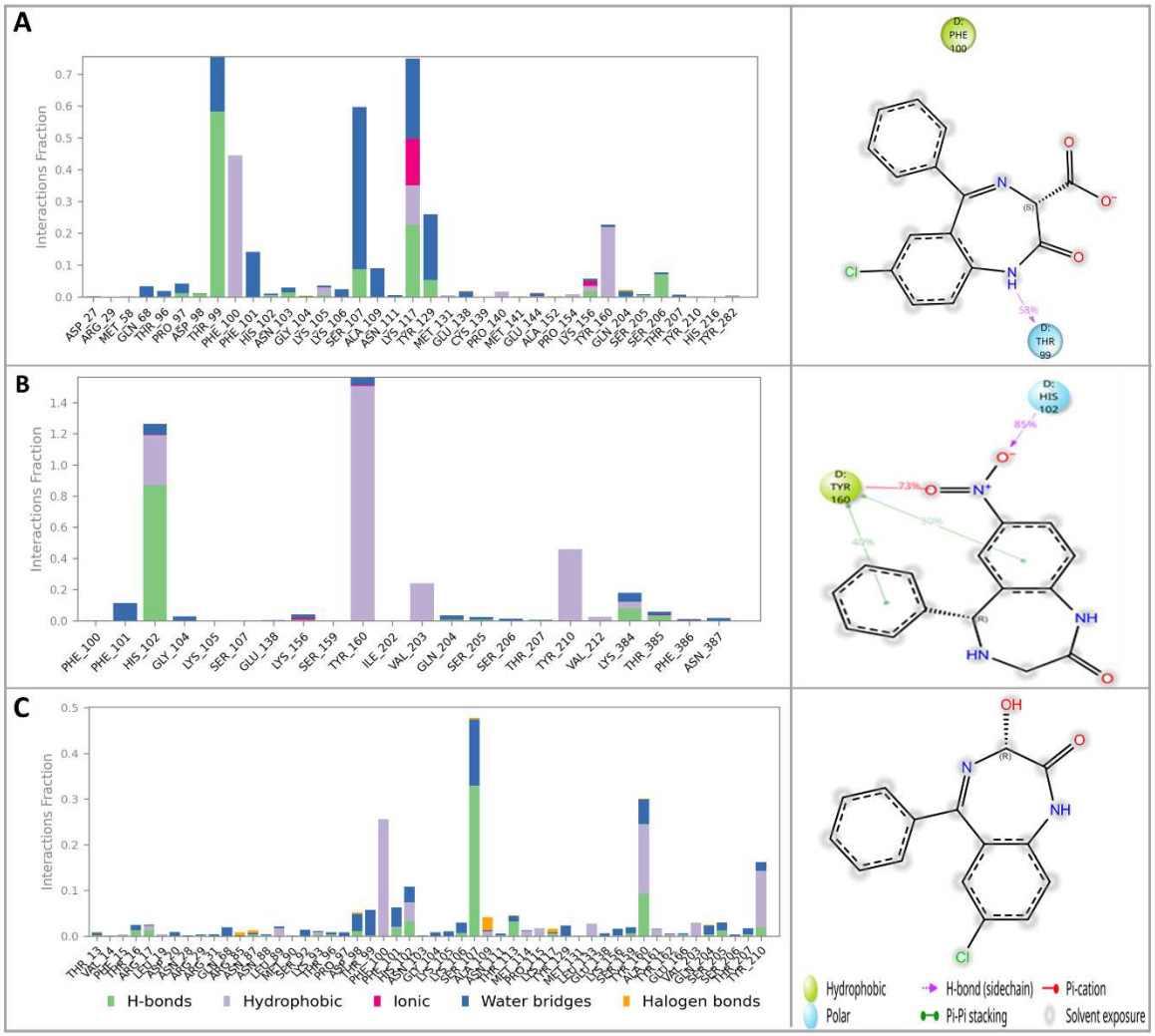


Figure 8. Protein–ligand interaction profiles of the selected complexes over 100 ns, shown as stacked bar charts for (A) CZP, (B) NZP, and (C) OXA.

989 **Table 1.** Predicted binding affinities and non-bonded interactions of the selected BZDs with
990 the isolated α1 subunit of the GABA-A receptor (PDB ID: 6HUO), including interacting
991 residues, interaction types, and distances.

Ligand	Binding affinity (kcal/mol)	Residue in contact	Interaction type *	Distance (Å)
ALP (Bound drug)	-7.5	SER205	H	2.674
		TYR210	PPS	3.905
		PHE100	PPTS	5.181
		TYR160	PPTS	5.504
		PHE100	PA	4.756
		TYR160	PA	4.768
TMZ	-6.8	SER205	H	2.958
		PHE100	PA	5.144
		TYR210	PPS	4.064
		PHE100	PPT	5.211
CDP	-6.8	THR207	H	2.229
		TYR160	PPS	5.183
		TYR210	PPS	4.202
		PHE100	PPTS	5.147
		TYR160	PPTS	5.238
		PHE100	PA	4.650
FZP	-6.2	SER205	H	2.523,
		TYR160	PA	4.869
		SER205	H	2.672
		TYR210	PPS	3.881
		TYR160	PPTS	5.674
		PHE100	PA	4.879
MDZ	-6.8	SER205	H	2.336
		TYR210	PPS	4.063
OXA	-7.3	SER205	H	2.092
		THR207	Psi	3.957
		TYR210	PPS	4.0091
		TYR160	PPTS	5.261
		TYR160	PA	5.487
CZP	-6.9	SER205	H	2.347
		TYR210	PPS	3.942
		PHE100	PPTS	5.238
		TYR160	PPTS	5.485
		PHE100	PA	4.823
		TYR160	PA	4.749
CBZ	-6.4	TYR160	H	2.691
		PHE100	PPT	5.050
		PHE100	PA	5.049
		HIS102	PA	4.120
		TYR160	PA	4.647
		TYR210	PA	3.916
		VAL203	PA	5.380
ESZ	-6.8	TYR210	PPS	4.026
		PHE100	PPTS	5.205
		PHE100	PA	5.422
CLZ	-6.6	HIS102	H	2.274
		TYR160	H	2.518
		HIS102	PdH	3.045
		PHE100	PPT	4.884
		PHE100	PPT	5.150
NZP	-7.1	HIS102	H	2.055
		SER205	H	2.698
		PHE100	PPTS	4.675
		VAL203	PA	5.027

992 * PA: π-Alkyl, H: Conventional hydrogen bond, PdH: π-Donor hydrogen bond, Psi: π-Sigma, PPS: π-π Stacked,
993 PPTS: π-π T-shaped.

Table 2. The three selected complex average RMSD, RMSF, and Rg.

Parameter	CZP	NZP	OXA
Protein Cα RMSD (Å)	4.67±1.145	4.31±0.938	4.57±0.729
Ligand RMSD (Å)	13.79±3.779	5.12±0.538	25.59±22.960
Protein Cα RMSF (Å)	1.98±1.095	2.21±1.077	1.83±0.934
Radius of gyration (Å)	3.62±0.026	3.50±0.028	3.55±0.029
Solvent-accessible surface area (Å^2)	274.92±70.626	216.17±19.915	306.028±119.989
Hydrogen bond	1.11±0.832	1.01±0.490	1.11±1.032

Table 3. PASS-predicted biological activities of the selected benzodiazepines.

Compounds	Pharmacological Activity (Pa values)						
	Anti-neurotic	Muscle relaxant	Anti-convulsant	Anxiolytic	GABA receptor agonist	Anti-epileptic	CYP3A4 Substrate
TMZ	0.527	0.954	0.947	0.927	0.877	0.574	0.635
CDP	0.44	0.494	0.698	0.626	-	-	-
FZP	0.924	0.986	0.967	0.742	0.806	0.715	0.729
MDZ	0.891	0.964	0.923	0.799	0.727	0.731	0.409
OXA	0.527	0.891	0.934	0.913	0.822	0.721	0.704
CZP	0.815	0.756	0.852	0.477	0.526	0.508	0.327
CBZ	0.555	0.448	0.891	0.684	0.695	0.561	0.575
ESZ	0.88	0.664	0.939	0.849	0.918	0.725	0.604
CLZ	0.464	0.817	0.905	0.41	0.664	0.582	0.728
NZP	0.505	0.736	0.847	0.382	0.563	0.507	0.695

Table 4. Predicted absorption, distribution, metabolism, excretion, and toxicity (ADMET) properties of the selected BZDs.

Name	Absorption				Distribution	Metabolism		Toxicity			
	BBB	HIA	CP	P-GpS	SL	CYP450 3A4	CYP450 2C9	hERG	C	TPT	AOT
OXA	+0.964	+0.983	+0.887	-0.517	0.589(M)	0.656(NI)	0.506(NI)	0.873(NI)	0.771	0.990(hTPT)	0.727(III)
CLZ	+0.898	+0.993	+0.500	-0.763	0.467(M)	0.639(I)	0.606(NI)	0.889(NI)	0.780	0.969(hTPT)	0.469(III)
TMZ	+0.975	+0.991	+0.798	-0.550	0.622(M)	0.601(NI)	0.545(NI)	0.831(NI)	0.809	0.934(hTPT)	0.814(III)
CDP	+0.837	+0.929	+0.591	-0.560	0.605(M)	0.833(NI)	0.756(NI)	0.921(NI)	0.659	0.942(hTPT)	0.613(III)
ESZ	+0.980	+1.000	+0.843	-0.594	0.662(M)	0.682(NI)	0.822(I)	0.894(NI)	0.713	0.985(hTPT)	0.807(III)
CBZ	+0.991	+0.990	+0.749	-0.573	0.459(M)	0.701(I)	0.530(NI)	0.865(NI)	0.785	0.940(hTPT)	0.620(IV)
CZP	+0.972	+0.995	+0.531	-0.560	0.452(N)	0.557(I)	0.521(I)	0.873(NI)	0.642	0.985(hTPT)	0.485(IV)
NZP	+0.980	+0.993	+0.518	-0.589	0.534(M)	0.679(I)	0.613(NI)	0.850(NI)	0.720	0.919(hTPT)	0.745(III)
FZP	+0.990	+1.000	+0.612	-0.855	0.611(M)	0.635(I)	0.711(NI)	0.718(I)	0.760	0.974(hTPT)	0.783(III)
MDZ	+0.972	+1.000	+0.887	-0.507	0.473(M)	0.521(NI)	0.713(I)	0.738(NI)	0.770	0.976(hTPT)	0.733(II)

*BBB Blood–Brain Barrier, HIA Human Intestinal Absorption, CP Caco-2 Permeability, P-GpS P-glycoprotein Substrate, SL Subcellular Localization, M Mitochondria, N Nucleus, C Carcinogens, TPT Tetrahymena pyriformis Toxicity, AOT Acute Oral Toxicity, NS Non-Substrate, NI Non-inhibitor, I Inhibitor, WI Weak-Inhibitor, NC Non-carcinogens, lTPT Low TPT, hTPT High TPT.